IEEE Access
Multidisciplinary ⋮ Rapid Review ⋮ Open Access Journal

Received September 29, 2020, accepted October 11, 2020, date of publication October 29, 2020,
date of current version November 19, 2020.

Digital Object Identifier 10.1109/ACCESS.2020.3034741

Research on Factors Affecting the Imaging Resolution of Magneto–Acousto–Electrical Tomography

MING DAI[1,3], (Member, IEEE), JINFENG XU[1], TONG SUN[2], CHRISOPHER QIAN[3], MIAN CHEN[2], (Member, IEEE), XIN ZENG[2], SIPING CHEN[2], PENGHUI HAO[2], YUNFENG LI[2], YINGYING LIU[1], AND LIANGPING LUO[4]

[1]Department of Ultrasonography, Shenzhen People's Hospital, 2nd Clinical Medical College, Jinan University, Shenzhen 518020, China
[2]School of Biomedical Engineering, Health Science Center, Shenzhen University, Shenzhen 518060, China
[3]School of Biomedical Sciences, The Chinese University of Hong Kong, Hong Kong, China
[4]The First Affiliated Hospital, Jinan University, Guangzhou 510632, China

Corresponding authors: Jinfeng Xu (xuJinfeng@yahoo.com), Yingying Liu (yingyingliu@ext.jnu.edu.cn), and Liangping Luo (tluolp@jnu.edu.cn)

This work was supported in part by the Discipline Construction Capacity Improvement Project of Shenzhen Health and Family Planning Commission under Grant SZXJ2018014, and in part by the National Natural Science Foundation of China under Grant 81771841, Grant 91859122, Grant 81471735, and Grant 81971637.

ABSTRACT As the conductivities of healthy tissue and cancerous tissue are different, methods for detecting conductivity variations of biological tissue are potential medical imaging modalities for early diagnosis of cancer in the future. Magneto-acousto-electrical tomography (MAET) is a noninvasive and hybrid conductivity imaging technology that integrates the advantage of high contrast. It has been demonstrated to have an excellent capability to distinguish conductivity variations along the direction of acoustic propagation and extremely promising as an alternative medical imaging technology for early detection of cancer. However, the existing MAET has a low resolution, and the factors affecting the imaging resolution of MAET are rarely studied systematically. Therefore, we firstly designed an MAET detection system and performed several verification experiments. A B-scan algorithm was then proposed for enhancing the system resolution. Subsequently, two uniform phantoms with different intermediate gaps in the middle and a B-mode imaging experiment on pork tissue were used for testing the performance of detection resolution. Finally, comparative analyses were performed to verify whether the frequency, the cycle number of the excitation signal, and the B-scan algorithm can influence the detection resolution. We obtained the following results: 1) The longitudinal resolution of the conductivity B-scan image increases as the number of cycle excitation decreases. 2) Vertical resolution using a 2.5 MHz probe excitation is significantly better than using a 500 kHz probe excitation. 3) The B-scan algorithm can improve conductivity resolution, and it reveals that our proposed detection system's longitudinal resolution can reach 1mm. 4) we obtained the conductivity profile of pork tissue. The results showed that our detection platform could accurately distinguish the target sample's interfaces of conductivity variations, increasing the excitation frequency, reducing the cycle number, and adopting the B-mode imaging algorithm could improve its conductivity detection resolution, which laid the foundation for the design of a high-resolution MAET detection system.

INDEX TERMS Conductivity tomography, weak signal processing, magneto–acousto–electrical detection, electromagnetic interference.

I. INTRODUCTION

Numerous studies have found that conductivity variation within a tissue provides physiological information, reflects the pathological state of biological tissue, and that conductivity variation is a conspicuous feature of most cancer tissues in their early stage [1]. For instance, the conductivity of healthy breast tissues is much lower than that of breast cancer tissues, and the conductivity of muscle tissue is about ten times that of fat tissue [2]. Therefore, the conductivity difference can

The associate editor coordinating the review of this manuscript and approving it for publication was Rajeswari Sundararajan.

be employed as a sensitive sign for pathological diagnosis. Imagining the electrical impedance of both cancer tissues and surrounding healthy tissues may help the doctors diagnose cancer early and significantly reduce cancer mortality [3]. Thus, imaging the conductivity is likely to be one of cancer detection modalities in the future [1], which has attracted considerable attention among many biomedical tomography investigators, and several conductivity detection modalities intended to derive the conductivity distributions inside image object are being extensively investigated, like magnetic resonance electrical impedance tomography (MREIT) [4], [5], electrical impedance tomography (EIT) [6], magnetoacoustic tomography (MAT) [7], magnetic induction tomography (MIT), and acoustoelectric tomography (AET) [8]. However, the above-mentioned imaging methods have their limitations, for example, the spatial resolution of MIT methods is low, which limits its application [9], AET exists the nonlinear problems and its reconstruction algorithm is complex [10], the magnetoacoustic signal of MAT is challenging to be detected and processed, as for MREIT, a high level current injection is always needed and is may harmful to imaging tissue [11], and the detection resolution of EIT is strictly restricted by the electrical insulation of the imaging body and quantity of the electrodes [12].

Since magneto-acousto-electrical tomography (MAET) integrates the strong points of the acoustic, electric, and magnetic fields and advantages of both the traditional EIT and ultrasound imaging. Besides, the magneto–acousto–electrical (MAE) voltage signal collected via electrode pair is detected and processed conveniently [13], [14]. The method of increasing the acoustic beam's excitation frequency can easily enhance the detection resolution of MAET, which is useful for reducing the cost and complexity of the MAET detection systems [3]. Therefore, MAET is widely and intensively researched worldwide and may achieve widespread application [15], [16].

MAET is presented initially by Wen *et al.* [15] and also called Hall effect imaging [17]. In 2013, Grasland-Mongrain *et al.* [2] renamed MAET as Lorentz force EIT and designed an experimental apparatus for imaging animal gelatin [3]. In 2008, the formula of Lorenz force induced electrical signal produced in anisotropic biological tissue was obtained by Roth and Tseng [18]. The relationship among the acoustic pressure of the probe, electrical potential, and electrical property inside the target sample was investigated by Xu *et al.* [19], [20]. An MAET detection apparatus using sinusoid-Barker-coded excitation was designed, and clear MAE signals of a 3-layered animal gel imitation were derived by Yu *et al.* [21]. The MAE signal could distinguish conductivity variations along the ultrasonic beam direction, which was discovered by Ma *et al.* [3]. In 2020, a three-dimensional mathematical simulation model of MAET was presented, and a three-dimensional image was reconstructed by Li *et al.* [22]. Numerical simulation of multi-angle MAET for improving image reconstruction of MAET was presented by Sun *et al.* [23]. Furthermore, noninvasive modality of treatment-efficacy evaluation for high-intensity focused ultrasound ablation using MAET technology was theoretically investigated by Zhou *et al.* [24].

Although tremendous achievements were made in the past two decades, some issues need to be further investigated. [25] For instance, the theory of deconvolution was proposed by A. Montalibet *et al.*, but they did not reconstruct the conductivity image within the target sample [26]. P. Grasland-Mongrain obtained the MAET image of biological tissue for the first time in 2015. The image effect was unsatisfactory due to the non-uniform magnetic field and low ultrasonic stimulating frequency [27]. Numerical simulations and related imaging experiments on a multi-layered phantom and a pork tissue sample were conducted by Liu *et al.* [15]. However, a detailed study of the factors affecting the resolution of MAET has not yet been conducted.

Although the MAET system using the chirp signal excitation method was presented in our previous research, its application requires a broad bandwidth probe. The excitation signal with wide bandwidth imposes higher requirements for amplifying and detecting of MAE signal [14], [28]. Ma *et al.* further improved the theory of deconvolution and reconstructed the conductivity distribution of a 3-layered animal gel imitation, and proposed that the longitudinal resolution of the MAE signal is affected by the wavelength of the ultrasonic beam [3]. However, they have not yet conducted related experiments to verify the theory and analyze its effect on conductivity resolution. The detection resolution obtained by a 0.5 MHz probe is not good enough. The rotational reconstruction method for deriving the conductivity distributions inside the imaged object was employed to perform an MAET imaging experiment on a circular phantom and meat sample by L. Kunyansk *et al.* in 2017 [29]. However, the improvement of detection resolution was limited. Although Chen *et al.* first proposed a multi-focus MAET detection platform using chirp signal stimulation, it presented several effective methods to reduce the electromagnetic interference signal (EMI) and improve the resolution of the B-scan image. They also clarified that the number of cycles of the cosinusoidal stimulus signal is the main factor that affects the imaging resolution of MAET [16]. However, they have not been verified and analyzed the influence factor by experiments and have not yet been reported the conductivity B-mode image of biological tissue.

Since current MAET has a low detection resolution on biological tissue, the influences of the frequency, cycle number of the excitation signal and B-scan imaging algorithm on conductivity resolution of MAET have not been studied. It is of considerable significance to investigate the factors affecting the conductivity detection resolution of MAET. Therefore, in this study, we designed an MAET experimental platform, proposed a reconstruction B-scan algorithm that can be used for improving conductivity axial resolution, and explored the factors for improving the spatial resolution of conductivity. Besides, two uniform gel phantoms with

different intermediate gaps (3mm, 1mm) (4-layers conductivity change interfaces) and a real pork tissue were utilized for B-scan imaging experiments to verify the performance of our designed MAET system. The experiments illustrated that the detection resolution of our proposed MAET system could reach 1 mm, and the conductivity outline of the pork tissue was derived. The detected conductivity boundary was coincided with the thickness of the target imaging body, indicating the accuracy, effectiveness, and feasibility of our proposed MAET detection approaches and platform. It provided the possibility of the boundary measurement for cancers and the materials damage detection in the future.

II. IMAGING PRINCIPLE AND METHOD

A. IMAGING PRINCIPLE

In our MAET imaging platform, firstly, a short pulse stimulating signal is sent to an ultrasound transducer to produce vibration within the target sample. Then, the opposing Lorentz forces are generated under the action of a static magnetic field and ultrasonic beam. Then the negatively and positively charged particles are separated, creating an electric current perpendicular to the direction of the ultrasound and magnetic fields. Finally, producing a μ V-level MAE signal on the surface of the target imaging body, which is measured by a pair of electrodes attached to the lateral sides of the imaging sample. The imaging principle of MAET within a target sample is plotted in Fig. 1.

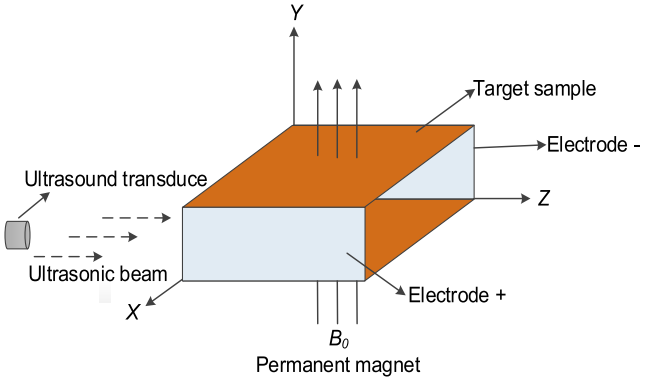

FIGURE 1. Imaging principle of MAET.

In the above imaging process, to simplify theoretical derivation, we make some ideal assumptions that ultrasound pressure is low enough without considering the nonlinear effect and ultrasound propagation in a fluid media without any viscosity and energy loss [3]. Consequently, the ultrasound pressure meets the linear inviscid force equation [30], and the vibration velocity at (z, t) can be described as

$$v(z,t) = -\frac{1}{\rho(z)} \int_0^t \frac{\partial p(z,t)}{\partial z} dt \tag{1}$$

Under the excitation of an acoustic beam, the vibration of ion occurs, the vibration velocity of a single charged ion q can be denoted as v. Due to the interaction with a static magnetic field B, ion deflection occurs by the induced Lorenz force $F = qv \times B$, which is perpendicular to the vibration velocity v and magnetic field B. The electrical potential along the x-axis is generated, establishing a time-varying electrical field source $E = v \times B$, which conversely forms a current density J within the imaging sample.

As the electrodes are placed on the x-axis, and the magnetic field is on the y-axis, the component of vibration velocity along the z-axis can be written as v_z. Thus, the current density can be described as

$$J_x = \sigma v_z \times \mathrm{B}_y \tag{2}$$

In practice, the net current is only a part of the total electric flow generated by the Lorentz force, so the fraction is set to μ and the impedance of the measurement system is denoted as R_0. Integrating J_x over the ultrasound path s and ultrasound beamwidth W. The received voltage can be expressed in the form of Eq. (3).

$$V(t) = \mu W R_0 B_y \int_s \sigma(z) v(z,t) dz \tag{3}$$

Substituting Eq. (1) into Eq. (3), the detected MAE voltage can be simplified as

$$V(t) = -\mu W R_0 B_y \int_s \frac{\sigma(z)}{\rho(z)} \left[\int_0^t \frac{\partial p(z,t)}{\partial z} dt \right] dz \tag{4}$$

As the imaging body is soaked in density uniform media, $\rho(z)$ can be simplified into ρ_0. Combining Eq. (4) by parts and supposing the stimulating acoustic beam transmits from position z1 to z2, the detected MAE signal can be rewritten as

$$\begin{aligned} V(t) = &-\frac{\mu W R_0 B_y \sigma(z)}{\rho_0} \int_{-\infty}^{t} p(z,t) dt \Big|_{z1}^{z2} \\ &+\mu W R_0 B_y \int_{z1}^{z2} \left(\frac{\partial}{\partial z} \left(\frac{\sigma(z)}{\rho_0} \right) \right) \int_{-\infty}^{t} p(z,t) dt \, dz \end{aligned} \tag{5}$$

Supposing the ultrasound momentum is expressed as $M(z,t) = \int_{-\infty}^{t} p(z,t) dt$, Eq. (5) can be expressed in the form of Eq. (6).

$$\begin{aligned} V(t) = &\frac{\mu W R_0 B_y}{\rho_0} \int_{z1}^{z2} \left(\frac{\partial \sigma(z)}{\partial z} \right) M(z,t)) dz \\ &-\frac{\mu W R_0 B_y \sigma(z)}{\rho_0} M(z,t) \Big|_{z1}^{z2} \end{aligned} \tag{6}$$

As the excitation signal is a cosinusoidal waveform, the integral of the ultrasonic excitation signal is equivalent to zero at any time of the interval encompassing the whole ultrasonic beam. In other words, the net momentum of the ultrasonic beam is zero [31]. Thus, the second term in Eq. (6) is zero when the ultrasonic wave packet propagates within the target sample, and the detected MAE signal can then be simplified as:

$$V(t) = \frac{\mu W R_0 B}{\rho_0} \int_{z1}^{z2} \left(\frac{\partial \sigma(z)}{\partial z} M(z,t) \right) dz \tag{7}$$

B. IMAGING METHOD

According to Eq. (7), the nonzero MAE signal only appears at the locations where a conductivity gradient exists [17]. In other words, as the wave packet of the ultrasonic beam passes through a conductivity variation interface, a weak Hall voltage is generated, and the total MAE voltage turns to nonzero. The detected MAE signal's peak implies the position of the conductivity variation interfaces of the target sample [17]. The peak time of each wave packet represents the interface position of the conductivity variation. Then, after scanning around an imaging body using an excitation probe, a reconstructed conductivity image of the target sample can be obtained by a B-scan imaging algorithm. The whole imaging principle is similar to that of B-mode ultrasonography. Therefore a B-mode image with relative conductivity information of the target sample can be derived by joining lots of MAE voltage signals at different stimulating locations with their positions information on the x-axis.

C. PLATFORM DESIGN

1) DETECTION SYSTEM DESIGN

To explore the influences of the ultrasonic excitation frequency, the number of excitation cycles, and B-scan imaging algorithm on conductivity imaging resolution and improve the imaging resolution of MAET, we designed and implemented an MAET measurement platform, which contained four components: 1) excitation and acquisition section, 2) transducer motion control section, 3) detection front end section and 4) data processing and imaging platform.

As a critical part of the MAET detection platform, the excitation and acquisition section consists of a function generator (AFG3102, Tektronics Inc., USA), a 53-dB power amplifier (RF Power A150, Electronics & Innovation Inc., New York, USA), a four-channel oscilloscope (DPO5054B, Tektronics Inc., USA), a custom-made and high-power single element transducer, two cascaded differential amplifiers (PXPA6, Pengxiang technology Inc., Hunan, China) and a homemade band-pass filter (-3 dB bandwidth 1 MHz). The detection front end section consists of silver-plated copper electrodes pairs, a C-shaped static magnet with two cube-shaped permanent magnets and corresponding support structure, and a measuring tank with the C-shaped static magnet inside. The transducer motion control section contains a planar ultrasound probe and a motion control device. The motion control device (MC600, ZOLIX Instruments Inc., Beijing, China) is employed for the movement of the stimulating transducer. A personal computer is utilized for data processing for the B-scan algorithm processing and conductivity imaging of offline MAE signals. The detection system block diagram and physical diagram are shown in Fig. 2 (a) and (b), respectively.

In our proposed MAET apparatus, a personal computer sends a control command and controls the motion controller's movement via an RS232 serial port. The signal generator is triggered by a motion controller to generate several cycles of the cosinusoidal excitation signal. The stimulating probe

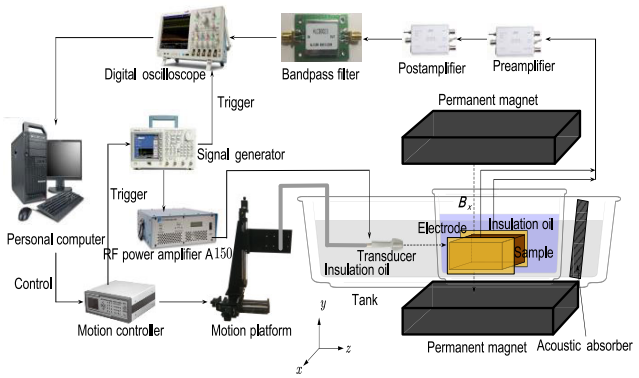

(a)

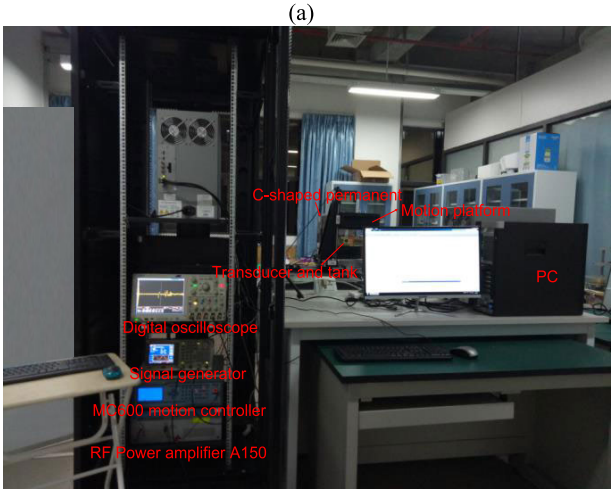

(b)

FIGURE 2. System composition of our proposed MAET system. (a) Connection block diagram. (b) Physical diagram.

is employed to produce the ultrasonic beam to cause local vibration of the target sample. Besides, two differential multistage amplifiers are utilized for amplifying the weak MAE signals. The silver-plated copper electrode pairs are linked to the differential pre-amplifier, and that electrode pairs are used to closely connect to both sides of the target sample. The C-shaped static magnet is utilized for yielding an approximate 0.78 T uniform magnetic field. Non-conductive oil is used as the coupling media between the transducer and imaging body, and a slanted ultrasonic absorbing baffle is employed as an acoustic absorber.

In our MAET detection, the excitation probe and the target sample are placed in the tank and soaked into insulating oil. A function generator generates a stimulating short pulse with a repetition time of 10 ms, 2-6 cycles of cosinusoidal waves, and 600 mV amplitude. After being amplified by the 53dB power amplifier, the stimulating signal is sent to drive an immersion-type transducer. A pair of electrodes is utilized to collect the MAE signal. An adjustable differential pre-amplifier (PXPA6, 10 dB, China) connecting to the electrode pairs is mainly applied for reducing

the common-mode interference, and an adjustable low-noise post-amplifier (PXPA6, 30 dB, China) is applied for secondary amplification. A homemade band-pass filter is used to improve the signal-to-noise ratio (SNR) of the MAE signal. After that, the MAE voltage is collected by the multi-channel oscilloscope at the 20-MHz sampling frequency. After being processed over 3000 times by mean filter, the oscilloscope displays and saves the MAE signal in CSV format. The collected MAE signal is further processed offline in a personal computer equipped with MATLAB 2015a. During the above imaging process, by moving the probe on the x-axis, repeating the above steps, and combining the MAE voltage signals with their location information, a B-mode image with conductivity information is derived after being processed by a B-scan imaging algorithm.

2) B-SCAN IMAGING ALGORITHM

The SNR of the MAE signal has a significant influence on the conductivity resolution. To derive a high SNR MAE signal and improve the conductivity B-mode image's detecting resolution, we proposed an effective conductivity B-mode imaging algorithm, analyzed and evaluated the influences that the B-scan algorithm on conductivity resolution. Firstly, in our B-scan algorithm, the surrounding noise is filtered out by the mean calculation (MC) for more than 3000 times. Then, Wiener filtering (WF) is used for further screening out the processed data, and Hilbert transform (HT) is performed to derive the envelope distribution of the MAE signal. Next, a B-mode scanning image with MAE voltage distributions is reconstructed after combining the processed MAE voltages at different stimulating locations with their corresponding x-axis position. Finally, a B-mode image with conductivity information is achieved by performing a linear interpolation algorithm. In this study, Wiener filtering is used to filter out the external noise and obtain high SNR of the MAE signal. Hilbert transform is utilized for deriving the envelope of the MAE voltages and turn the polarized wave packet of the MAE signal into a unipolar wave packet. The linear interpolation algorithm is applied to smooth the conductivity B-mode image for achieving a high-accuracy interface position of the conductivity variation.

III. EXPERIMENTS AND RESULTS

A. EFFECT OF CYCLE NUMBER OF EXCITATION SIGNAL ON DETECTION RESOLUTION

To explore the influences of the cycle number of excitation signal on detection resolution, we carried out a verification experiment. In that experiment, a uniform cuboid phantom was used as a target sample, and an ultrasonic beam with an excitation frequency of 2.5 MHz, three cosinusoidal pulses, a repetition frequency of 100 Hz and an amplitude of 600 mV was used as an excitation source. The collected MAE signal is shown in Fig. 3 (a), and then making sure the other conditions were unchanged, when the excitation signal cycle number increased from 3 to 6, the collected MAE signal could be seen

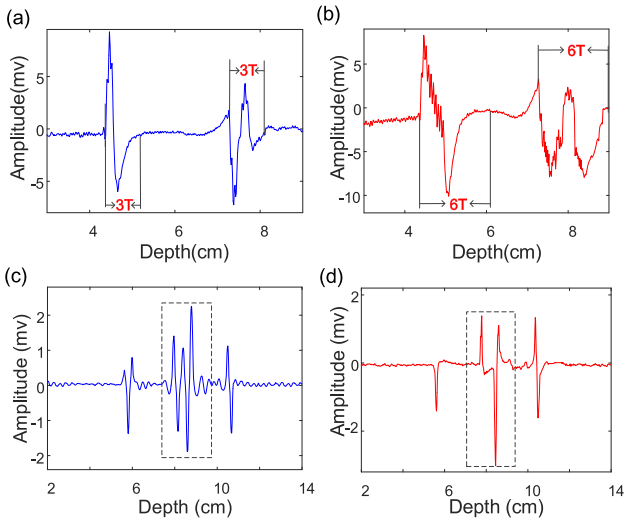

FIGURE 3. Study on factors affecting conductivity resolution. (a) The MAE signal collected when using a 3-cycle cosinusoidal excitation at 2.5 MHz as the excitation signal. (b) The MAE signal received when using a 6-cycle cosinusoidal excitation at 2.5 MHz as the excitation signal. (c) The MAE signal detected when using a 2-cycle burst at 500 kHz as the excitation signal. (d) The MAE signal collected when using a 2-cycle burst at 2.5 MHz as the excitation signal.

in Fig. 3 (b). From Fig. 3 (a) and (b), it is shown that the MAE signal using a 6-cycle cosinusoidal excitation at 2.5 MHz has significant ripple noise than using a 3-cycle excitation signal at 2.5 MHz. The width of the MAE wave packet received at the interfaces of the conductivity variation is related to the cycle number of the ultrasonic excitation signal. The more the excitation signal cycle number, the higher the excitation power, but the lower the detection resolution. The fewer cycles of the excitation signal, the higher the detection resolution, but the smaller the detection SNR.

B. EFFECT OF EXCITATION FREQUENCY ON IMAGING RESOLUTION

We used a uniform phantom with four conductivity variation interfaces as a target sample to explore the influences of excitation frequency on conductivity resolution in this article, and a 2-cycle ultrasonic stimulating burst of cosinusoidal pulses was generated and applied to the immersion-type probe. Under the same cycle number (2-cycle) of the excitation signal, comparative experiments were performed, and clear MAE signals were obtained after being processed by a Wiener filter. When the excitation frequency increased from 0.5 MHz to 2.5 MHz, the collected MAE signal was shown in Fig. 3 (c) and Fig. 3 (d). From Fig. 3 (c) and Fig. 3 (d), the detection resolution using an excitation signal with an excitation frequency of 2.5 MHz is significantly better than that of 0.5 MHz, which indicates that the higher the ultrasonic excitation frequency, the better the longitudinal detection resolution.

Moreover, as shown in Fig. 3, it also can be seen that the MAE wave packet's width is equal to the multiplication of cycle number and wavelength of the excitation signal.

TABLE 1. Accuracy analysis.

Items	MAEs processed by MC	MAEs processed by WF	MAEs processed by HT
Upper interface (cm)	14.19	14.19	14.22
Lower interface (cm)	17.11	17.05	17.05
Thickness (cm)	2.92	2.86	2.83
Accuracy (%)	95.8	97.9	98.9

It clarifies the cycle numbers and excitation frequency of the ultrasonic stimulating source directly affect the interface detection resolution of the conductivity variation. The fewer cycle numbers of the excitation signal and the higher the ultrasonic excitation frequency, the higher the detection resolution of the MAE signal. Therefore, to obtain a high SNR MAE signal and acquire a high detection resolution of a B-scan image, an ultrasonic excitation signal with two cycles of cosinusoidal pulses, an excitation frequency of 2.5 MHz was utilized as the ultrasonic excitation source in subsequent experiments.

C. INFLUENCE OF B-SCAN ALGORITHM ON IMAGING RESOLUTION

To derive a high accuracy of a B-mode image and further improve the detection performance of resolution, in this work, we proposed a B-scan imaging algorithm and carried out several comparative experiments. A uniform gel imitation with 0.5% salinity (7.5 × 2.8 × 3.5 cm) was placed in the middle of a detection tank and utilized as the imaging body to demonstrate the influence that the B-scan algorithm on imaging resolution. The target gel imitation is shown in Fig. 4 (a). After being processed by mean calculation, the detected MAE voltage signal is shown in Fig. 4 (b). As shown in Fig. 4 (b), the SNR of the MAE signal detected by our MAET measurement platform is high. The two interfaces of the conductivity variation can be recognized significantly. The average

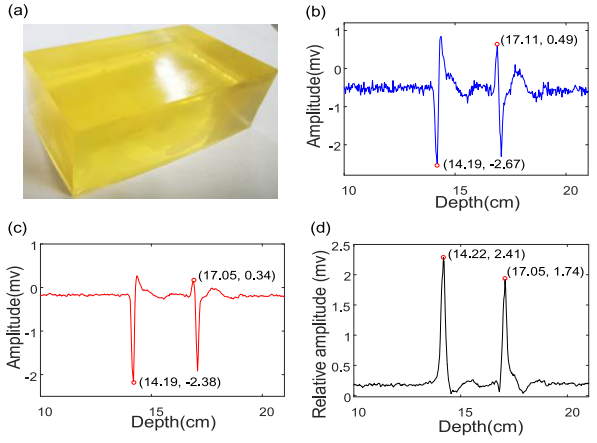

FIGURE 4. Influence of B-scan algorithm on detection resolution. (a) Target uniform phantom. (b) MAE signal processed by MC. (c) MAE signal processed by WF. (d) MAE signal processed by HT.

interface locations of the conductivity variation of the upper and lower imitation interfaces are close to 14.19 and 17.11 cm, respectively. Thus, the average thickness of the uniform phantom is approximately 2.92 cm, which illustrates that the width of the phantom calculated by the MAET detection system is close to the actual value (2.8 cm) measured by ultrasound imaging, the detection accuracy of the uniform phantom is shown in Table 1.

Besides, to improve the detection resolution, in this work, Wiener filtering was applied to cut down external noise interference in our study. The obtained MAE waveform after being processed by Wiener filtering was shown in Fig. 4 (c), from which we can see that Wiener filtering significantly reduces external noise interference, and the SNR and detection resolution of the MAE signal is much high. The two obtained interface positions of conductivity change are 14.19 and 17.05 cm, and the calculated thickness of the imitation is 2.86 cm, which demonstrates that Wiener filtering can improve the detection resolution. Subsequently, to further enhance the imaging resolution, Hilbert transform processing was performed on the above MAE signal to derive the envelope of the MAE wave packet at each excitation position, and the processed MAE signal by HT is shown in Fig. 4 (d). As shown in Fig. 4 (d), the two peak positions of the two envelopes of the MAE signal are 14.22 and 17.05 cm, respectively, and the calculated thickness of the uniform imitation is 2.83 cm, with the measured value being much closer to the actual 2.8 cm thickness of the phantom, indicating that the B-scan imaging algorithm including MF, WF, and HT is suitable for interface measurement of the conductivity change area and can improve detection resolution of conductivity.

To achieve the conductivity distribution of MAET in a planar area, we conducted a scanning motion experiment to perform stepscan movements along the x-axis. After the probe is moved to scan the uniform phantom along the x-axis direction, the MAE signals at different excitation positions are received and recorded. Then the recorded data is processed by MC, WT, HT, and two-dimensional linear interpolation algorithm. A B-mode image containing the information of conductivity discontinuity distribution within the target phantom is reconstructed after combing the MAE signals with the probe's excitation position.

D. TEST EXPERIMENT OF DETECTION RESOLUTION

To measure the detection resolution in the longitudinal direction and to investigate the characteristics of the MAE voltage, specific softbox and fixture were applied to make an imitation

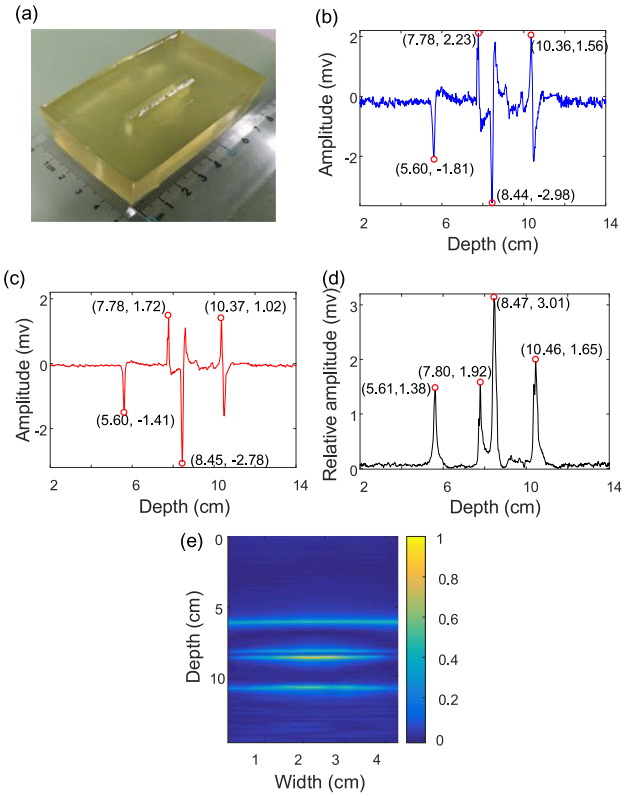

FIGURE 5. Vertical resolution experiments. (a) Target phantom with a narrow slit width of 3 mm. (b) MAE signal processed by mean filtering. (c) MAE signal processed by a Wiener filtering. (d) MAE signal processed by a Hilbert transform. (e) A reconstructed B-scan image of the phantom with a narrow slit width of 1 mm.

(7.5 × 4.85 × 3.2 cm), with a thickness of 4.85 cm, a middle slit length of 3.5 cm and a narrow slit width of 3 mm, as shown in Fig. 5 (a). The stimulating probe was fixedly installed in the center of the left side of the target imitation, and the ultrasonic beam passed through the target sample with four conductivity change interfaces. Finally, our proposed detection system performed an accuracy test of two uniform phantoms with a different narrow slit width (1mm and 3 mm). The conductivity curve obtained by measuring the uniform phantom with a slit width of 1 mm is shown in Fig. 5 (b). Four interface locations of electrical conductivity change can be seen clearly, and the four detected interface locations of the target imitation are consistent with the actual interface positions.

Subsequently, WT in the time domain was carried out for the above conductivity curve, and the MAE signal processed by WT is as shown in Fig. 5 (c). The obtained MAE signal after the HT is then shown in Fig. 5 (d). The intermediate slits measured in the above experiments are 0.66, 0.67, and 0.67 mm, respectively, close to the 1 mm narrow slit width measured before the test. The above experimental differences are mainly caused by the expansion and deformation of the target phantom in the insulating oil, which also demonstrates the high accuracy of our proposed MAET measurement platform.

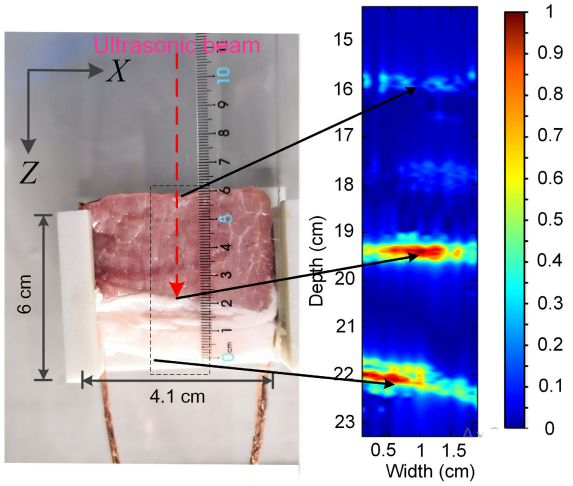

FIGURE 6. B-scan imaging experiment on a pork tissue.

In this study, we carried out the stepscan movements along the x-axis for 45 times to derive a B-mode image with conductivity information, with the step-size was set as 1 mm. Then, 45 MAE signals were obtained and processed by the B-mode scanning algorithm, and a reconstructed B-mode conductivity image of the uniform phantom with a narrow slit width of 1 mm is shown in Fig. 5 (e). As shown in Fig. 5 (e), the result proves that our designed MAET detection system's longitudinal detection resolution on a uniform phantom can reach 1mm.

E. B-SCAN IMAGING EXPERIMENT OF PORK TISSUE

Additionally, a conductivity B-scan imaging experiment on a pork sample with layered fat and lean tissue was carried out by applying MC, WF, HT, and 2D interpolation processing. The tested pork tissue (approximately 41 × 60 mm) and a reconstructed B-mode image with electrical conductivity distribution are shown in Fig. 6. From which the interface locations of conductivity change of the pork tissue can be roughly distinguished.

The measured profile is consistent with the actual interface locations of conductivity change of the pork tissue, demonstrating the feasibility of the conductivity measurement method and revealing that our designed MAET detection platform and imaging algorithm can measure the interfaces of conductivity changes. Although a clear B-scan image of the uniform phantom is achieved, the SNR of the pork tissue's B-mode reconstruction image is still low. Therefore, more robust imaging algorithms and effective detection methods against external noise are needed to improve the conductivity resolution further.

IV. DISCUSSION

MAET is a noninvasive and developing conductivity detection modality that merges the advantages of the magnetic, electromagnetic, and acoustic fields. To obtain high SNR of

the MAE signal and explore factors affecting the conductivity resolution of MAET, in this work, an enhanced MAET measurement system was designed and implemented, and the simplified MAET equations were supplied. Moreover, uniform phantom and real biological tissue experiments were conducted to test the MAET detection system's performance, and comparative analyses were performed to explore factors that affect conductivity resolution. The relative measurement errors and methods improving conductivity resolution have been analyzed and evaluated. As shown in Fig. 3 (a) and (b), the cycle number of excitation signal affects the width of the wave packet of the excitation signal, and excessive cycle numbers of the excitation signal cause overlap between adjacent wave packets, thereby reducing the spatial resolution of the MAET detection system. In Fig. 3 (c) and (d), the detection resolution of the MAE signal obtained by an excitation frequency of 2.5 MHz is significantly better than that obtained by an excitation frequency of 0.5 MHz, which shows that the excitation frequency has a significant influence on the waveform and detection resolution of the MAE signal.

As shown in Fig. 4 and Table 1, the B-scan algorithm improves the SNR of the MAE voltage, MC, WF, and HT gradually improve the MAE signal's detection accuracy to some extent. The accuracy of the uniform phantom experiment was up to 95%. Besides, the four-layered uniform phantom with interface a narrow slit width of 1 mm was used to evaluate the detection resolution of our MAET measurement platform and explore the characteristics of the MAE signal, as shown in Fig. 5, the wave packet of the MAE signal only appears at the interface positions where a conductivity variation occurs. The amplitude and vibration polarity of the wave packet represents the value and direction of conductivity variation. After being processed by the MC, WF, HT, and linear interpolation algorithm, a four-layered B-mode image with conductivity information, such as the location of conductivity variation, the relative amplitude of conductivity can be reconstructed, as shown in Fig. 5 (e), with the longitudinal detection resolution of the conductivity B-mode image of the target phantom capable of reaching 1mm.

The B-scan image of real biological pork tissue demonstrates that the MAET measurement platform can obtain the interface position of the conductivity change of biological tissue, and the detected interface positions coincide with the pork tissue profiles. Although we achieved the profile of the pork tissue, the obtained detection resolution is not high. The main reasons may be as follows: 1) The conductivity difference (insulating oil, 0.5% NaCl) at the interface position of 0.5% NaCl regular phantom varies greatly, the conductivity difference between lean and fat, and the conductivity difference between lean/fat and insulating oil are much smaller than the conductivity variation between insulating oil and 0.5% NaCl, that is to say, the conductivity in the pork tissue experiment has a small range of change, which results in a low detection sensitivity. 2) In this work, 18 step movements with a 1 mm step length are carried out in the X-axis direction, which affects the lateral resolution. The lateral resolution is also affected by the three-dimensional motion platform. Moreover, the scale calibration between the horizontal axis and the vertical axis is different in figure 6. 3) In order to ensure sufficient excitation energy, a planar power probe with a diameter of about 2 cm was used to excite the target sample in our MAET detection platform, it means that the ultrasonic beamwidth is about 2 cm, which results in low lateral resolution and detection sensitivity of conductivity. Although the excitation frequency, the number of excitation cycles, and the conductivity B-scan algorithm can improve the longitudinal resolution of MAET, those methods still cannot improve the lateral resolution of conductivity. 4) The shape (regular, irregular) of the target sample has a significant influence on the longitudinal resolution of MAET. The measured target sample is an irregularly layered porcine tissue with low conductivity variation. Those may be the main reasons why the reconstructed boundaries are almost in parallel, and the sloping boundary of the porcine tissue is not displayed clearly in Fig. 6. Besides, although the pork tissue's three interface profile can be derived with a very poor resolution in the horizontal direction, it is not yet possible to accurately image the conductivity change interfaces of pork tissue. Thus, the MAET detection system and imaging methods for real biological tissue need to be optimized and improved further. Additionally, current research on the MAET detection system and factors affecting the spatial resolution are in their early stages. The conductivity measurement approach and its experimental setup need to be further enhanced. Although some achievements were made, the detection resolution of the pork tissue's conductivity B-mode image is still limited and needs improvement. Thus, further investigations are required to optimize the MAET detection platform, such as adopting ultrasonic coding technologies, designing an ultra-low noise detection apparatus, and adding nanoparticles into the target sample (enhance the detection sensitivity), using a magnetic shielding probe. A single sinusoid signal, rather than a more complex ultrasonic stimulating signal such as barker coded signal, pseudo-random coded signal, and chirp pulse wave, was utilized as the excitation signal. Therefore, more effective digital coding methods and a complicated stimulating signal are required for further study. Additionally, the transducer is only performed step motion on the x-axis in our experiments, the horizontal resolution is restricted by step length, and the low imaging speed means it is hard to achieve real-time imaging. Therefore, the electronic delay focusing method using a multi-array linear array probe can significantly improve the imaging speed and detection accuracy to some extent.

V. CONCLUSION

In this article, a noninvasive MAET detection system with a short pulse signal stimulation was designed and implemented. Experiments exploring conductivity resolution factors were performed on two different uniform phantoms and real natural pork tissue. The influences that the stimulating pulse's number and excitation frequency on conductivity resolution was analyzed and discussed by experiments.

The corresponding results revealed that the proposed MAET measurement platform could accurately distinguish the target imaging body's conductivity variation interfaces, and the B-mode imaging algorithm was demonstrated experimentally to be able to improve the conductivity detection resolution. Additionally, the conductivity B-mode image of a uniform gel imitation with an intermediate slit of 1 mm was obtained clearly. It showed the interface positions of conductivity variation, which showed an agreement with the actual phantom interface positions. The 1mm slit within the target phantom could be distinguished clearly, proving the feasibility, effectiveness, and precision of the MAET detection platform. It also demonstrated that the detection resolution of our MAET detection system could reach 1mm. Finally, the pork tissue profile was derived by performing a B-scan experiment on a multilayer pork tissue; the conductivity interface positions detected by our B-scan imaging method were precise. It was in agreement with the profiles of the imaging body, which indicates that our MAET modality has the potential to be an alternative biomedical imaging method for cancer diagnosis and the identification of cancerous tissue in the future. Although the uniform phantom experiments proved that our proposed MAET detection platform could achieve a high detection resolution of the target phantom, the real biological sample's conductivity imaging resolution is not satisfactory. It demonstrates that the MAET detection system still needs to be further enhanced. Therefore, it is necessary to carry out verification experiments on non-uniform phantoms, cancer tissues embedded in uniform phantoms, and cancer tissues to explore more effective methods for improving the conductivity resolution in biological tissues, which will be the emphasis of our next study.

COMPETING INTERESTS

The authors report no conflicts of interest.

REFERENCES

[1] D. Haemmerich, S. T. Staelin, J. Z. Tsai, S. Tungjitkusolmun, D. M. Mahvi, and J. G. Webster, "*In vivo* electrical conductivity of hepatic tumours," *Physiol. Meas.*, vol. 24, no. 2, pp. 251–260, 2003.

[2] P. Grasland-Mongrain and C. Lafon, "Review on biomedical techniques for imaging electrical impedance," *IRBM*, vol. 39, no. 4, pp. 243–250, Aug. 2018.

[3] Y. Zhou, Q. Ma, G. Guo, J. Tu, and D. Zhang, "Magneto-acousto-electrical measurement based electrical conductivity reconstruction for tissues," *IEEE Trans. Biomed. Eng.*, vol. 65, no. 5, pp. 1086–1094, May 2018.

[4] O. F. Oran and Y. Z. Ider, "Magnetic resonance electrical impedance tomography (MREIT) based on the solution of the convection equation using FEM with stabilization," *Phys. Med. Biol.*, vol. 57, no. 16, pp. 5113–5140, Aug. 2012.

[5] M. Chauhan, W. C. Jeong, H. J. Kim, O. I. Kwon, and E. J. Woo, "Optimization of magnetic flux density for fast MREIT conductivity imaging using multi-echo interleaved partial Fourier acquisitions," *Biomed. Eng. OnLine*, vol. 12, no. 1, p. 82, 2013.

[6] B. Brown, "Electrical impedance tomography (EIT): A review," *J. Med. Eng. Technol.*, vol. 27, no. 3, pp. 97–108, Jan. 2003.

[7] Y. Xu, and B. He, "Magnetoacoustic tomography with magnetic induction (MAT-MI)," *IEEE Trans. Med. Imag.*, vol. 29, no. 10, pp. 1759–1767, 2010.

[8] X. Song, Y. Zhou, R. S. Witte, and D. Ming, "Noninvasive acoustoelectric imaging of resistivity distribution based on lead field theory," *IEEE Trans. Instrum. Meas.*, vol. 68, no. 12, pp. 4779–4786, Dec. 2019.

[9] K. Yu, Q. Shao, S. Ashkenazi, J. C. Bischof, and B. He, "*in vivo* electrical conductivity contrast imaging in a mouse model of cancer using high-frequency magnetoacoustic tomography with magnetic induction (hfMAT-MI)," *IEEE Trans. Med. Imag.*, vol. 35, no. 10, pp. 2301–2311, Oct. 2016.

[10] C. Li, K. An, and K. Zheng, "The Levenberg–Marquardt method for acousto-electric tomography on different conductivity contrast," *Appl. Sci.*, vol. 10, no. 10, p. 3482, 2020.

[11] Y. Song, J. K. Seo, M. Chauhan, A. Indahlastari, N. Ashok Kumar, and R. Sadleir, "Accelerating acquisition strategies for low-frequency conductivity imaging using MREIT," *Phys. Med. Biol.*, vol. 63, no. 4, 2018, Art. no. 045011.

[12] D. S. Holder, "Electrical impedance tomography: Methods, history and applications," *Med. Phys.*, vol. 32, no. 8, p. 2731, 2005.

[13] A. S. Rekhi and A. Arbabian, "Remote sub-wavelength focusing of ultrasonically activated lorentz current," *Appl. Phys. Lett.*, vol. 110, no. 16, Apr. 2017, Art. no. 164104.

[14] M. Dai, X. Chen, M. Chen, H. Lin, F. Li, and S. Chen, "A novel method to detect interface of conductivity changes in Magneto-Acousto-Electrical tomography using chirp signal excitation method," *IEEE Access*, vol. 6, pp. 33503–33512, 2018.

[15] Y. Li, G. Liu, H. Xia, and Z. Xia, "Numerical simulations and experimental study of Magneto-Acousto-Electrical tomography with plane transducer," *IEEE Trans. Magn.*, vol. 54, no. 3, pp. 1–4, Mar. 2018.

[16] M. Dai, X. Chen, T. Sun, L. Yu, M. Chen, H. Lin, and S. Chen, "A 2D Magneto-Acousto-Electrical tomography method to detect conductivity variation using multifocus image method," *Sensors*, vol. 18, no. 7, p. 2373, Jul. 2018.

[17] H. Wen, J. Shah, and R. S. Balaban, "Hall effect imaging," *IEEE Trans. Biomed. Eng.*, vol. 45, no. 1, pp. 119–124, Jan. 1998.

[18] N. Tseng and B. J. Roth, "The potential induced in anisotropic tissue by the ultrasonically-induced lorentz force," *Med. Biol. Eng. Comput.*, vol. 46, no. 2, pp. 195–197, Feb. 2008.

[19] Y. Xu, S. Haider, and A. Hrbek, "Magneto-acousto-electrical tomography: A new imaging modality for electrical impedance," in *Proc. 13th Int. Conf. Elect. Bioimpedance 8th Conf. Elect. Impedance Tomogr.* Berlin, Germany: Springer, 2007, pp. 292–295.

[20] S. Haider, A. Hrbek, and Y. Xu, "Magneto-acousto-electrical tomography: A potential method for imaging current density and electrical impedance," *Physiol. Meas.*, vol. 29, no. 6, pp. S41–S50, Jun. 2008.

[21] Z. F. Yu, Y. Zhou, Y. Z. Li, Q. Y. Ma, G. P. Guo, and J. Tu, "Performance improvement of magneto-acousto-electrical tomography for biological tissues with sinusoid-Barker coded excitation," *Chin. Phys. B*, vol. 27, no. 9, 2018, Art. no. 0943021.

[22] Y. Y. Li, J. X. Song, H. Xia, Y. H. Li, and G. Q. Liu, "Three-dimensional model of conductivity imaging for magneto-acousto-electrical tomography," *J. Appl. Phys.*, vol. 127, no. 10, 2020, Art. no. 104701.

[23] T. Sun, X. Zeng, P. Hao, C. Ting Chin, M. Chen, J. Yan, M. Dai, H. Lin, S. Chen, and X. Chen, "Optimization of multi-angle Magneto-Acousto-Electrical tomography (MAET) based on a numerical method," *Math. Biosci. Eng.*, vol. 17, no. 4, pp. 2864–2880, 2020.

[24] Y. Zhou, Z. Yu, Q. Ma, G. Guo, J. Tu, and D. Zhang, "Noninvasive treatment-efficacy evaluation for HIFU therapy based on Magneto-Acousto-Electrical tomography," *IEEE Trans. Biomed. Eng.*, vol. 66, no. 3, pp. 666–674, Mar. 2019.

[25] M. Dai, T. Sun, X. Chen, L. Y. Yu, M. Chen, and S. P. Chen, "A B-scan imaging method of conductivity variation detection for magneto–acousto–electrical tomography," *IEEE Access*, vol. 7, pp. 26881–26891, 2019.

[26] A. Montalibet, J. Jossinet, and A. Matias, "Scanning electric conductivity gradients with ultrasonically-induced lorentz force," *Ultrason. Imag.*, vol. 23, no. 2, pp. 117–132, Apr. 2001.

[27] P. Grasland-Mongrain, F. Destrempes, J. M. Mari, and R. Souchon, "Acousto-electrical speckle pattern in Electrical Impedance Tomography," *Inst. Phys. Eng. Med.*, vol. 60, no. 9, pp. 3747–3757, 2015.

[28] Z. Sun, G. Liu, H. Xia, and S. Catheline, "Lorentz force electrical-impedance tomography using linearly frequency-modulated ultrasound pulse," *IEEE Trans. Ultrason., Ferroelectr., Freq. Control*, vol. 65, no. 2, pp. 168–177, Feb. 2018.

[29] L. Kunyansky, C. P. Ingram, and R. S. Witte, "Rotational magneto-acousto-electric tomography (MAET): Theory and experimental validation," *Phys. Med. Biol.*, vol. 62, no. 8, p. 3025, 2017.
[30] L. Kunyansky, "A mathematical model and inversion procedure for magneto-acousto-electric tomography," *Inverse Problems*, vol. 28, no. 3, pp. 35002–35022, 2011.
[31] H. Wen, E. Bennett, J. Shah, and R. S. Balaban, "An imaging method using the interaction between ultrasound and magnetic field," in *Proc. IEEE Ultrason. Symp. Int. Symp.*, vol. 10, Oct. 1997, pp. 1407–1410.

MING DAI (Member, IEEE) received the B.S. degree in computer science and technology from Hainan Tropical Ocean University, Sanya, Hainan, in 2012, the M.S. degree in electronics and communication engineering from Nanchang Hang kong University, Nanchang, Jiangxi, and also from the Shenzhen Institutes of Advanced Technology, Chinese Academy of Sciences, Shenzhen, Guangdong, in 2015, and the Ph.D. degree in information and communication engineering from Shenzhen University, Shenzhen, Guangdong, in June 2019. From 2019 to 2020, he was a Visiting Scholar with The Chinese University of Hong Kong. He is currently holds a postdoctoral position with Jinan University and study in Shenzhen People's Hospital, 2nd Clinical Medical College, Jinan University. His research interests include electrical conductivity imaging, biomedical multimodal data fusion, image processing, artificial intelligence, things engineering, big data technology and application, wearable medical applications, and the design of electrical systems.

JINFENG XU received the M.D. degree in imaging medicine and nuclear medicine imaging medicine and nuclear medicine from the Tongji Medical College, Huazhong University of Science and Technology, in 2009. In 2009, he joined as a Doctor with the Department of Ultrasonography, Shenzhen People's Hospital. He was a Visiting Scholar with Oregon Health Sciences University. He is currently a Chief Physician and the Director of the Department of Ultrasonography, Shenzhen People's Hospital, and also a Professor and a Doctor Supervisor with the Second Clinical Medical College, Jinan University. His research interests include the ultrasound diagnosis of abdominal, thyroid, breast, and peripheral vascular diseases. He participated in the development of national guidelines for ultrasound diagnosis of thyroid and breast.

TONG SUN received the B.S. degree in biomedical engineering from Northeastern University, China, in 2016. He is currently pursuing the Ph.D. degree in learning and scientific research with Shenzhen University. His research interests include medical ultrasonic imaging and biomedical conductivity imaging.

CHRISOPHER QIAN received the M.S. degree in biomedical engineering from The Chinese University of Hong Kong, in 2017, where he is currently pursuing the Ph.D. degree. His research interests include data analysis, decision making, cognition, and motivation.

MIAN CHEN (Member, IEEE) received the Ph.D. degree in analytical chemistry from Hunan University, China, in 2014. He is currently an Associate Researcher with the School of Biomedical Engineering, Shenzhen University. His research interests include using functional nanomaterials for cancer diagnosis and treatment.

XIN ZENG received the B.S. degree in biomedical engineering from Southern Medical University, China, in 2016. He is currently pursuing the M.S. degree in biomedical engineering with Shenzhen University, Shenzhen, China. His research interests include medical ultrasonic imaging and biomedical conductivity imaging.

SIPING CHEN received the Ph.D. degree in biomedical engineering from Xi'an Jiaotong University, Shanxi, China, in 1987. After a postdoctoral fellowship at Zhejiang University, Zhejiang, China, he joined Shenzhen Anke High-tech Co., Ltd., as a Chief Technology Officer in 1989. Having served at Anke for 16 years, he joined Shenzhen University as the Vice President and founded the Biomedical Engineering Branch, Shenzhen University, in 2005. His current research interests include biomedical ultrasound imaging, medical instrumentation, tissue elasticity imaging, multimodal ultrasound imaging, and image processing.

PENGHUI HAO received the B.S. degree in biomedical engineering from Zhengzhou University, China, in 2017. He is currently pursuing the M.S. degree in biomedical engineering with Shenzhen University, Shenzhen, China. His research interests include medical ultrasonic imaging and biomedical conductivity imaging.

YUNFENG LI received the bachelor's degree in electrical engineering and the master's degree in signal detection in 2016 and 2019, respectively. He is currently pursuing the Ph.D. degree with Shenzhen University. His research interests include the Internet of Things technology, artificial intelligence, image processing, wearable smart devices, and blockchain.

YINGYING LIU received the M.D. degree in imaging medicine and nuclear medicine imaging medicine and nuclear medicine from the Tongji Medical College, Huazhong University of Science and Technology, in 2010. She was a Visiting Scholar with Cleveland Clinic, USA, in 2016. She is currently an Associate Chief Physician with the Department of Ultrasonography, Shenzhen People's Hospital, and also an Associate Professor and a Master's Supervisor with The Second Clinical Medical College, Jinan University. Her research interests include cardiovascular ultrasound and molecular imaging.

LIANGPING LUO received the M.S. degree in imaging medicine and nuclear medicine from Jinan University, in 1991. He is currently pursuing the Ph.D. degree with Humboldt University, Germany. In 1991, he joined as a Doctor with the Department of Medical Imaging, The First Affiliated Hospital, Jinan University. In June 2000, he held a postdoctoral position with Jinan University, where he became a Professor. He is also a Ph.D. Tutor. His research interests include the comprehensive imaging diagnosis of thoracic diseases, especially lung cancer and pleural tumors and the study of molecular biology basis.